Title
Metabolites of Cannabigerol Generated by Human Cytochrome P450s Are Bioactive

Journal
Biochemistry, 61(21)

ISSN
0006-2960

Authors
Roy, Pritam
Dennis, David G
Eschbach, Mark D
et al.

Publication Date
2022-11-01

DOI
10.1021/acs.biochem.2c00383

Peer reviewed

HHS Public Access

Author manuscript

Biochemistry. Author manuscript; available in PMC 2023 July 12.

Published in final edited form as:

Biochemistry. 2022 November 01; 61(21): 2398–2408. doi:10.1021/acs.biochem.2c00383.

Metabolites of Cannabigerol (CBG) Generated by Human Cytochrome P450s are Bioactive

Pritam Roy[†,‡], **David G. Dennis**[†,a,b], **Mark D. Eschbach**[‡], **Shravanthi D. Anand**[‡], **Fengyun Xu**[c], **Jonathan Maturano**[a,b], **Judith Hellman**[c], **David Sarlah**[*,a,b], **Aditi Das**[*,‡,b]

[‡]Department of Comparative Biosciences, Center for Biophysics and Quantitative Biology, Beckman Institute for Advanced Science and Technology, Department of Bioengineering, Neuroscience program, University of Illinois Urbana-Champaign, Urbana IL 61801, School of Chemistry and Biochemistry, Georgia Institute of Technology, Atlanta, Georgia 30332, United States.

[a]Roger Adams Laboratory, Department of Chemistry, University of Illinois, Urbana, Illinois 61801, United States

[b]Cancer Center at Illinois, University of Illinois, Urbana, Illinois 61801, United States

[c]Department of Anesthesia and Perioperative Care, University of California San Francisco San Francisco, CA.

Abstract

The phytocannabinoid cannabigerol (CBG) is the central biosynthetic precursor to many cannabinoids, including Δ^9-tetrahydrocannabinol (THC) and cannabidiol (CBD). Though the use of CBG has recently witnessed a widespread surge because of its beneficial health effects and lack of psychoactivity, its metabolism by human cytochrome P450s is largely unknown. Herein, we describe comprehensive *in vitro* and *in vivo* cytochrome P450 (CYP)-mediated metabolic studies of CBG, ranging from LC-MS/MS-based primary metabolic site determination, synthetic validation, and kinetic behavior using targeted mass spectrometry. These investigations revealed that cyclo-CBG, a recently isolated phytocannabinoid, is the major metabolite that is rapidly formed by selected human cytochrome P450s (CYP2J2, CYP3A4, CYP2D6, CYP2C8, and CYP2C9). Additionally, *in vivo* studies with mice administered with CBG, supported these studies, where cyclo-CBG is the major metabolite as well. Spectroscopic binding studies along with docking and modeling of CBG molecule near the heme in the active site of P450s confirmed these observations, pointing at the preferred site-selectivity of CBG metabolism at the prenyl chain over other positions. Importantly, we found out that CBG and its oxidized CBG metabolites reduced inflammation in BV2 microglial cells stimulated with LPS. Overall,

[*]**Corresponding Author**: Aditi Das, Ph.D. University of Illinois Urbana-Champaign, 3836 VMBSB, 2001 South Lincoln Avenue, Urbana IL 61802, Phone: 217-244-0630. aditidas@illinois.edu, David Sarlah Ph.D. University of Illinois Urbana-Champaign, 270 RAL, Box 107-5, 600 South Mathews Avenue Urbana IL 61801, Phone: 217-244-9154. sarlah@illinois.edu.
[†]The authors have contributed equally

The authors declare no competing financial interest.

Supporting Information
The Supporting Information is available free of charge on the ACS Publications website.
Detailed experimental procedures, spectroscopic data, ^{1}H and ^{13}C NMR spectra (PDF), docking studies and detailed discussions are provided.

combining enzymological studies, mass spectrometry, and chemical synthesis, we showcase that CBG is rapidly metabolized by human P450s to form oxidized metabolites that are bioactive. The study reveals the structure-activity relationship of CBG metabolites and analogs to their anti-inflammatory activity.

Graphical Abstract

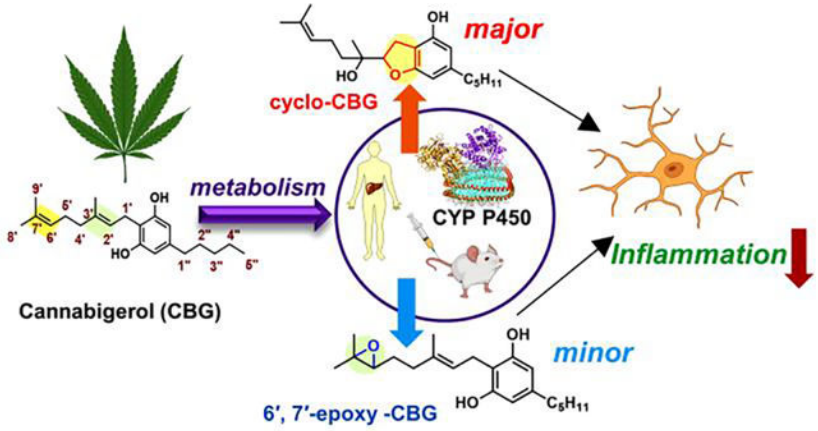

INTRODUCTION

Cannabigerol (CBG, **1**, Figure 1) is often referred to as the mother of phytocannabinoids (pCBs) since most of the pCBs in the cannabis plant, including Δ^9-tetrahydrocannabinol (Δ^9-THC, **3**) and cannabidiol (CBD, **4**) are synthesized from the related cannabigerolic acid (CBGA, **2**).[1] Phytocannabinoids demonstrated beneficial effects in the treatment of pain, cancer, asthma, and arthritis,[2–4] and while most research has been focused on major constituents Δ^9-THC and CBD, CBG is increasingly being used for medicinal purposes owing to its non-psychotropic behavior and wide range of pharmacological effects.[5] It was postulated that CBG mimics the endocannabinoids due to its versatility in physiological function;[6] however, conclusive mechanistic work is still required in this regard. Recent studies have shown that CBG interacts weakly with the cannabinoid receptors (CBR1 and CBR2),[7,8]is the most potent ligand of transient receptor potential (TRPV1) among the phytocannabinoids,[9] and can also activate α2 adrenoceptor (α2-AR).[10] Recently it has been found that CBG administration in C57BL/6J male mice can reduce blood pressure through α2-AR mechanism.[11] However, unlike CBD or THC, CBG exhibits a unique interaction with 5-hydroxytryptamine (5-HT_{1A}), associated with neuronal firing and release of neurotransmitter.[12] Moreover, CBG is known to exhibit anti-pain properties without any psychotropic side effects.[13] In humans, CBG proved effective in human inflammatory bowel diseases[5] and, similar to eicosanoid - epoxyeicosatrienoic acids (EETs), CBG reduces the eye pressure in glaucoma.[14] CBG is neuroprotective in Huntington's disease and is effective against methicillin-resistant *Staphylococcus aureus* MRSA.[15,16] Overall, there is potential that CBG will maintain the homeostasis in the body when the endocannabinoid system is disrupted in different diseases states.[13]

Structurally, CBG is monocyclic, containing linear prenyl chain, and is unique among pCBs which are polycyclic, as exemplified with Δ^9-THC and CBD (Figure 1). Consequently, the molecular pharmacology of CBG differs drastically; for example, the prenyl chain plays a crucial role in interacting with the amino acid residues and stabilizing the compound in the protein pocket of the aldose reductase (ALR2) enzyme which is involved in diabetic complications.[17] Interestingly, the prenyl chain is also required for the antibacterial activity, attributed to its ability to interact with the hydrophobic lipid membrane of bacteria.[18]

Since popularity and public use of CBG is gaining momentum,[19] more studies related to this natural product are needed; in particular, not much is known about the metabolism of CBG by cytochrome P450s (CYP) and pharmacology of its resulting metabolites. Metabolites often display different or even more potent bioactivities than their parent compounds. This has been shown with other major class of cannabinoids; for example, the CYP metabolite 11-hydroxyl-Δ^9-THC is more psychotropic than Δ^9-THC,[20,21] and CYP metabolites of CBD have shown different pharmacological effects than CBD itself.[22] Therefore, in the view of CBG's therapeutic potential, in-depth metabolic studies are crucial for complete evaluation of pharmacological profile and for development of novel CBG-based leads for treatment of conditions related to inflammation, pain, or abnormal cell proliferation.[23,24] Both the prenyl and the pentyl chains could be potential sites of metabolism for CYP enzymes. Indeed, previous *in vitro* work, involving microsome samples from different species and using GC-MS analysis, pointed that biotransformations occurs at multiple sites at the prenyl and pentyl chains.[25] Higher levels of 6′,7′-epoxide **5** formation and allylic hydroxylation products (C-8 and C-9) were obtained in species like mouse, rat, guinea pig, cat, and rabbit, indicating the higher preference of metabolism at the prenyl chain site. Interestingly, another constitutional isomer, **6**, was also detected, albeit, in smaller quantities. However, due to the lack of authentic standards, oxidized products predicted from the mass spectrometry fragmentation pattern could not be validated.[26,27,28] Therefore, it is pertinent to conduct a more holistic study on the metabolism of CBG by cytochrome P450s using synthesized authentic standards, as well as to evaluate their pharmacology for development of therapeutics. This study will reveal the structure-activity relationship of CBG metabolites and analogs to their anti-inflammatory activity.

CYPs are often involved in lipid metabolism and steroidogenesis within the body.[29,30] In the case of major pCBs, different subclasses of CYPs are involved in their metabolism. For example, the CYPs identified in metabolism of THC are mainly CYP2C9 and CYP2C11,[31,32] whereas CYP2D6 and CYP3A4 are involved in metabolism of CBD[33]. CBG has also been shown to cross the blood brain barrier[34] and regulate the appetite.[35] Hence it is important to study the metabolism of CBG in the presence of different classes CYPs present in humans that are present in liver (CYP3A4, CYP2C9, CYP2C8, and CYP2D6) and brain (CYP2J2 and CYP2D6).[36]

The two most common subtypes of CYP reactions are hydroxylation and epoxidation.[37] The epoxides are generally electrophilic and are prone to modify DNA or proteins. The epoxides undergo rapid hydrolysis into diols mediated by epoxide hydrolases.[38] Theoretical investigations using cytochrome P450 have been executed to understand the mechanism of epoxide formation by CYPs and how the structural properties of a drug determine the

extent of epoxidation.[39,40] Herein, we investigate the binding and kinetics of epoxidation of CBG in the presence of recombinantly expressed human CYPs. While CYP3A4, CYP2D6 and CYP2C9 are predominant drug-metabolizing CYPs, CYP2C8 and CYP2J2 are CYPs in the endothelium, cardiovascular system that are known to function as epoxygenases.[41] In this study, we showcased that CBG is metabolized by human CYPs *in vitro* and by mouse CYPs *in vivo* to form two major metabolites, cyclo-CBG (**7**) and 6′,7′-epoxy-CBG (**5**) as shown in Figure 1. Interestingly, the cyclo-CBG (**7**) is a minor phytocannabinoid that was found in high-potency *Cannabis sativa*,[42] and 6′,7′-epoxy-CBG (**5**) is a putative precursor to carmagerol.[43] These CBG metabolites and several analogs (sesqui-CBG, carmagerol and 2′,3′-dihydroxy-CBG) were chemically synthesized to further understand the structure-function relationship of their bioactivity. Additionally, we develop targeted metabolomics methods to measure the oxidized metabolites using the synthesized standards and demonstrate the enzyme kinetics of the CYP-mediated CBG metabolism. Finally, we measure the bioactivity of the metabolites and their CBG analogs and show that all of them are bioactive in an anti-inflammatory assay utilizing microglial cells. Taken together, these fundamental studies in this work will help direct further studies towards the development of CBG-based therapeutics and understand structure-activity relationships of CBG metabolites and analogs.

RESULTS

Synthesis of CBG, its metabolites, and analogs.

In order to delineate the metabolism of CBG by the different human CYPs and to evaluate their bioactivity, we synthesized several potential metabolites (Figure 2). Thus, efforts were placed on preparation of both epoxides, as double bonds are often prone to rapid epoxidation. Moreover, the initial shotgun metabolomics involving CBG (**1**) with selected CYP and human liver microsome incubations (*vide infra*) identified 6′,7′-epoxy-CBG (**5**) and cyclo-CBG (**7**) as potential compounds of interest for further validation (Figure 2, S2, and S3). Since CBG contains reactive resorcinol core, prone to oxidation and reaction with electrophilic reagents, we first protected it as diacetate (**1**→**8**). Though two trisubstituted olefins are present in intermediate **8**, the survey of electrophilic reagents revealed a high chemoselectivity preference for 6′,7′-double bond. Thus, epoxidation with equimolar amounts of *m*CPBA, followed by acetate deprotection, delivered the desired 6′,7′-epoxy-CBG (**5**). Moreover, epoxide hydrolysis in the presence of perchloric acid furnished carmagerol (**9**). To oxidize the least reactive 2′,3′-double bond in **8**, we opted for the stepwise olefin masking, by first converting the most reactive olefin to the corresponding bromohydrin acetate (**8**→**10**), followed by epoxidation and conversion of bromohydrin acetate into an olefin (**10**→**11**). With protected 2′,3′-epoxy-CBG **11** in hand, we were able to obtain the cyclo-CBG (**7**) through deprotection and concurrent spontaneous cyclization. Though several deprotection conditions on intermediate **11** were attempted, as well as using different protecting groups (i.e., TBS); the intermediate 2′,3′-epoxy-CBG (**6**) was never observed. Interestingly, the cyclo-CBG (**7**) was isolated from *Cannabis sativa* and initially mischaracterized as a six-membered pyran-type compound;[42] however, careful analysis of NMR data agree with the structural revision to compound **7** that was recently provided based on computational predictions (See SI for details).[44] In addition to the preparation

of cyclo-CBG (**7**), we sought to prepare the corresponding diol **12** for detection as a potential metabolite. This was accomplished using acid-mediated hydrolysis followed by basic deprotection of acetoxy groups.

Direct metabolism of CBG by human CYPs determined using Liquid Chromatography -Mass Spectrometry.

Phytocannabinoids are metabolized by CYPs in the body within a few hours of consumption.[45] To study the metabolism of CBG by human liver microsomes (HLM), a LC-MS/MS method was established. In our present study, CBG metabolites were separated based on the structure and elution time (Figure 3A). The present study primarily focuses on the formation of epoxides in unsaturated bonds of the prenyl chain, which leads to the production of 2′,3′- and 6′,7′-epoxides (**6** & **5**). Epoxides of lipids such as anandamide (AEA) often display anti-inflammatory bioactivity.[46] The 2′,3′-epoxides are formed enzymatically but they cyclize spontaneously in the experimental conditions to form cyclo-CBG (**7**). Direct metabolism of CBG using human liver microsomes (HLM) analyzed using LC-UV followed by MS (Figure 3A) was compared with the chromatograms of standard cyclo- and 6′,7′ epoxy-CBG (Figure S3) followed by analysis of the mass spectra. Fragmentation pattern (Figure 3A1 and 3A2) indicated that the metabolites eluted at 4.6 min and 8.2 min corresponds to 6′,7′-epoxy and cyclo-CBG, respectively.

Furthermore, *in vivo* study was done in mouse by performing intravenous (IV) or intraperitoneal (IP) injections of CBG and quantifying the products in plasma. Both cyclo-CBG (**7**) and 6′,7′-epoxy-CBG (**5**) are detected in the plasmas from CBG treated mice. The amount of cyclo-CBG (**7**) is found to be ~100 times more than 6′,7′-epoxy-CBG (**5**) (Figure 3C, 3D and 3E). Metabolite formation is more predominant in the initial stages (0.5 h), however it decreases significantly after 2 h which points towards secondary metabolism of cyclo-CBG (**7**) and 6′,7′-epoxy-CBG by cytochrome P450s (**5**). The CBG concentration in blood after 0.5 h is ~700 ng/mL and after 2 h is ~60 ng/mL which comes to ~0.5–0.7 μM and ~0.05 μM respectively. However, the concentration of cyclo-CBG and 6′,7′ epoxy-CBG formed detected after 0.5 h were 1.5 μM and 7.5 nM respectively.

Anti-inflammatory assay using microglial cells to study the role of CBG in controlling inflammation.

Microglia are resident macrophages in the brain and spinal cord. They respond to injury, damage, or inflammation in the brain in myriad ways by secretion of cytokines and chemokines. Here, we used the BV2 microglial cell line and stimulated them with LPS to evoke an inflammatory response, and studied the expression of specific markers such as nitric oxide, IL-6, IL-10 in the presence and absence of CBG-based metabolites: CBG, 2′,3′-dihydroxy CBG (12), cyclo-CBG (7), pre-carmagerol (5), and carmagerol (9). The concentration of CBG and its metabolites are varied from 0–5 μM for this study. Previous studies have shown that levels of cannabinoids obtained in human blood plasma ranges in low micromolar range (e.g. ~0.06 μM for THC, and ~0.14 μM for CBD after 0.5 h). [47] This implies that tissue levels of these cannabinoid on administration can reach medium micromolar range. Therefore, previous cellular assays have been carried out in presence of 0–15 μM CBD concentration using carcinoma (HNSCC) cells.[48] Herein, the CBG based

compounds tested for LPS-induced cytotoxicity by lactate dehydrogenase (LDH) assay did not show any increase in % LDH release when used within a concentration range of 0–5 μM (Figure S7). A significant reduction in nitric oxide levels was observed for some of the CBG analogs; CBG (64.1±5.9) and carmagerol (60.0±6.03) exhibiting the highest reduction in % NO level indicating an anti-inflammatory activity (Figure S8). Furthermore, we quantified the levels of IL-6 and IL-10 by ELISA (Figure 3F and 3G). Among the CBG analogs tested, CBG (414.2±75.2) and carmagerol (307.8±159.1) showed a decrease in IL-6 expression at 5 μM concentration. Similarly, the levels of IL-10 showed an increase with 236.03±12.35 and 159.5±16.7 for CBG and carmagerol respectively. Overall, the study showed that CBG and its analogs and metabolites are anti-inflammatory in LPS-stimulated microglial cells. Previously it has been reported that epoxyeicosatrienoic acids (EETs) are anti-inflammatory that are formed by metabolism of arachidonic acid by CYPs.[46] In this present case lowering in IL-6 expression observed in presence of epoxy derivative of CBG (6′,7′-epoxy-CBG) which is formed from CYPs and carmagerol.

Metabolism of CBG by different liver CYPs.

To further understand the mechanism of formation of the specific CYP metabolites, 6′,7′-epoxy CBG (**5**) and cyclo-CBG (**7**), we studied the metabolism of CBG with specific CYPs: CYP2J2, 3A4, 2D6, 2C9 and 2C8, and pooled HLM (Figure 4). In these studies, CYP-CPR lipid reconstituted or nanodisc system were incubated with CBG in presence of NADPH, and the rate of formation of the products with change in concentration was used to calculate the maximum velocity (V_{max}) and K_m using standard Michaelis-Menten kinetics (Figure 4). Due to limited solubility in an aqueous solution; the CBG concentration was kept below 100 μM in these studies. The kinetics of the formation of cyclo-CBG (**7**) and 6′,7′-epoxy CBG (**5**) were compared among the four types of CYPs. The detection and quantification of CBG metabolites were carried out using HPLC coupled to a triple quadrupole detector, which enabled a highly sensitive, accurate, and reproducible method for detection of cyclo- and 6′,7′-epoxy CBG. The rate of cyclo-CBG formation was found to be at least 100 times higher as compared to that of 6′,7′-epoxide for all the CYPs studied (Figure 4). The cyclo-CBG formation is more prominent for 3A4 and 2C9 followed by 2J2 (Figure 4K) among the CYPs. Although 6′,7′-epoxy-CBG is the minor metabolite, CYP2J2 and CYP3A4 has comparatively higher amount of the epoxide product (Figure 4L). On the other hand, the rate of CBG metabolism in presence of 2C8 and 2D6 are almost 5–6 times slower as compared to 2C9. The higher preference for cyclo-CBG for 3A4 over 6′,7′-epoxy-CBG when compared to 2C9 indicates that catalytic activity of CYPs also depend on the type of product formed. The affinity of CBG for product formation (K_m) is also compared among five different CYPs (Figure S4). K_m value for CYP2J2 is found to be the highest and almost 1.5–2 times more than 2D6 and 2C8 for the formation of cyclo-CBG product. The K_m for cyclo-CBG formation for 2C9 and 3A4 is similar. Interestingly, the affinity for CBG towards the formation of the cyclo-CBG as well as 6′,7′-epoxy-CBG is much higher for 2D6 and 2C8 as compared to 2C9 and 3A4, but the catalytic activity of the former two CYPs are much lower as obtained from the V_{max} values. The data signifies that a single substrate has unequal affinities towards the same enzyme during the formation of different products. However, the affinity for the substrate towards multiple product formation cannot be completely explained by taking their K_m values, when multiple binding sites may be

available. Among the CYPs, the rate of product formation for 3A4, 2C9 and 2J2 does not strictly follow the Michaelis-Menten equation. Rather a sigmoidal growth is an indication of multiple site binding/binding of more than one ligand at the same time.[49,50] This was further explored by comparing the ratios of the rate of cyclo-CBG and 6′,7′-epoxy CBG over the range of CBG concentrations used (Figure S5). For CYP 3A4, 2C8, and 2C9 the ratio increases, whereas for 2D6, the opposite trend is observed. Unlike these CYPs, CYP2J2 does not show any specific trend. Although the ratio of cyclo-CBG is higher than 6′,7′-epoxy CBG, but the ratio varies with change in concentrations.

Spectral Competitive Binding Studies of CBG with different CYPs.

In order to delve into the binding interactions of CYPs with CBG, we measured CBG binding to CYPs using UV-visible spectroscopy. The heme group in CYPs is coordinated to a water molecule in the axial position, which on ligand binding is displaced leading to shift in the Soret band (~417 nm) towards ~393 nm, forming a high-spin iron complex. The magnitude of this spectral shift is plotted against the concentration of the ligand and is fitted to a binding equation in order to obtain a value of Ks, the spin-state equilibrium constant, which determines the binding efficiency of the ligand with CYPs. Initially, the direct binding of CBG to different CYPs was studied by varying the concentration of CBG from 0–75 μM (Figure 5A). CBG produces a blue shift in the Soret peak thus acting as a Type I ligand (Figure S1). The difference in absorbance between 393 nm and 417 nm was used to plot the binding curve (Figure 5A) and the Ks and ΔAmax values were obtained. Among all the CYPs, CBG shows the tightest binding to CYP2J2, which is almost three times greater than that of CYP2D6 and CYP2C8 (Figure 5B). The ΔAmax is higher for CYP2C8 even though it shows weaker binding with CBG compared to other CYPs (Table S1).

Furthermore, competitive binding assays using known substrates for the CYPs were used to confirm the above direct binding studies. The drugs specific to a particular CYP were added to CBG bound CYP that subsequently displaced CBG from the active site of the protein, thereby producing a more robust shift in the Soret band. This competitive binding was used to monitor the type of CYP inhibition by CBG and calculate the inhibition constant (Figure 5C). The substrates that were used to probe drug binding are the following: ebastine (EBS) for CYP2J2, testosterone (TST) for CYP3A4, thioridazine (TDZ) for CYP2D6 (TDZ), and retinoic acid (RTA) for CYP2C8. The binding curves of the CYPs with CBG as well as the corresponding drug were fitted into Michaelis-Menten or Hill binding models from where the Amax and K_s values were calculated (Table S1 and S2). For the competitive binding assay, CBG was found to produce an inhibition in the range of 10–20 μM for CYP2D6 and CYP3A4.

Docking studies to gain atomistic details of CBG binding to the CYPs.

To understand the atomistic details of binding of CBG to the CYPs, protein-ligand docking studies were performed. The study was carried out specifically by selecting the region near the active site of the protein. Autodock Vina gave nine docked poses with different conformations at the active site. For CYP2J2, CBG has been found to be distributed over multiple positions at the protein pocket (Figure S1B). However, for other CYPs, CBG is mainly located over the heme moiety, with either the prenyl or the pentyl chain facing the Fe

atom (Figure 5D and 5E and Figure S1B). The most energetically stable structure is shown in bold, whereas others are in thin wire for respective CYPs. The closest distance between CBG and Fe atom of CYPs were calculated to compare with the experimentally obtained binding affinity from the subtracted Soret spectra. It is observed that CBG is surrounded by both polar and non-polar residues within a radius of 5 Å. Key residues like Phe and Arg are present in all the docked structures, which signifies that CBG can interact both through π-stacking as well as electrostatic interaction owing to its phenolic moiety. These residues also play an important role in binding the substrate in specific orientations that can lead to site-specific metabolism depending on the CYPs used. However, the metabolism experiment shows a preferential selection of cyclo-CBG as a major metabolite over 6′,7′-epoxy-CBG in both *in vitro* and *in vivo* studies. This indicates that chemical properties of the substrate are more predominant in regulating the metabolism process compared to the substrate binding in the CYP active site. In order to understand this, CBG was docked with Fe-oxo (Cpd I) and the distances between the sites of metabolism were calculated from the oxygen atom connected to heme (Figure S1B). CBG adopts a bent structure in presence of Cpd I with C-2 being closer to the oxygen atom of heme as compared to C-6. This conformation is possible owing to the -OH functional group of CBG which can associate with Cpd I through H-bonding (Figure S1B(D)). Previously it has been shown that hydrogen bonding between the heme-oxo complex (compounds I) and the –OH groups of 1/2-naphthol is critical for the proton transfer process at the active site.[51]

DISCUSSION

Phytocannabinoids undergo biotransformation to form bioactive metabolites.[52,53] Herein, we study the CYP mediated metabolism of CBG, which is an important non-psychotropic cannabinoid with numerous health benefits. The binding affinity of CBG towards different human CYPs using direct and competitive binding studies in the presence of a specific CYP substrate was studied (SI Notes on Binding). The binding affinity for CBG towards CYP2J2 is the tightest among all the CYPs.[54,55,56] Competitive binding of EBS to CYP2J2-CBG bound complex increases the Ks by ~4 fold, implying that the presence of CBG reduces the affinity of EBS towards CYP2J2. This indicates that CBG occupies the same binding pocket as EBS in CYP2J2 and a higher concentration of EBS is required to displace CBG from the center as supported by docking studies that show Arg117, Ile376, and Val370 are the common binding site residues for both CBG as well as EBS.[57] The binding shows a single binding site in CYP2J2 for both EBS and CBG. Unlike CYP2J2, the Ks value is almost 3 times higher for CYP2C8 and CYP2D6 in presence of CBG, indicating comparatively weak binding to the protein. Binding studies indicate that CYP2C8 has at least 2 binding sites in the protein-based on n>1 hill coefficient (Figure S1A). Addition of RTA to CBG-bound CYP increases the Ks (~1.3 times) and ΔAmax (~1.2 times), suggesting comparatively lower inhibition of CYP2C8 by CBG, which is likely due to the fact that RTA and CBG separately bind to two different pockets in CYP2C8. Docking studies show that CBG occupies one of the binding pockets where RTA also binds to CYP2C8 and is stabilized by amino acid residues like Leu208. The Ks for CBG binding to CYP2D6 is almost 3.5 times lower than TDZ binding (substrate for CYP2C8). The CYP2D6 crystal structure shows that the protein exists in closed and open conformation with one and two molecules of TDZ attached to it,

respectively.[58] Here we show that CBG is localized near the heme group and can associate with Asp301 through polar interaction such as hydrogen bonding in CYP2D6 like that of TDZ from the crystal structure (Figure 5E). This indicates that CBG binds to a similar pocket as TDZ and prefers a closed CYP2D6 structure over open conformer. CYP3A4 shows stronger binding to CBG as compared to CYP2C8 and CYP2D6. TST, a substrate[59] for CYP3A4, binds almost 5 times more strongly as compared to CBG. CYP3A4-mediated TST metabolism suggested the importance of Ser119 which interacts with the substrate through hydrogen bonding.[60] The docked structure of CYP3A4 with CBG shows that it binds near the heme with residues like Ser119, Ala370, and Leu482, situated within 5 Å from CBG (Figure S1B(C)). This suggests that CBG binds to a common active site pocket in CYP3A4 similar to TST and midazolam. The docked structures of different CYPs bound to CBG (Table S3), show that the closer proximity of the CBG molecule towards heme promotes effective binding and reduces Ks values (SI-notes on binding). Displacement of the distal water molecule to the heme by the ligand produces a spin-state change that is reflected in the ΔAmax value. CYP2C8 produces the maximum spin-state change; however, it is situated at a higher distance from the heme (Table S3). Previously it has been shown that the Thr residue (present in the I-helix) in the mammalian CYPs is involved in stabilizing the water molecule coordinated to the heme group. CBG has an –OH group that can interact with the nearby polar residues such as Thr in the I-helix of the CYPs.[61] This interaction can affect the hydrogen bonding association between Thr and distal water molecule of Fe. Upon analyzing the distance between CBG and Thr in different CYPs, CBG is closest to the Thr301 residue for CYP2C8 (Table S4). However, this distance is comparable for CYP2J2 and 2D6 but higher in CYP3A4. This distance of the CBG to the Thr is proportional to the ΔAmax observed in our experimental data where CYP2C8 shows highest ΔAmax followed by CYP2J2, CYP2D6, and CYP3A4. This indicates that CBG can indirectly cause the spin-state change by interacting with the Thr residue of the protein.

The metabolism of CBG by the CYP P450s identifies the regions of the molecule that is transformed by the CYPs. Multiple factors can contribute to the rate of CBG metabolism: (i) substrate binding to CYPs, (ii) CYP-CPR interactions, and (iii) rate of electron flow from NADPH to CPR to CYP. CBG can be metabolized at multiple sites as previously observed with liver microsomes from different species.[25] Using human liver microsome (HLM) to study the metabolism of CBG, we show that two major products are formed from HPLC-MS (Figure 3A) where one peak corresponds to the formation of 6′,7′-epoxy CBG (Figure S2) and the other peak to the formation of 5 membered cyclo-CBG instead of 2′,3′-epoxy CBG(SI Notes on Metabolism). This study confirms the formation of 6′,7′-epoxy-CBG and cyclo-CBG as major metabolites during CBG metabolism by HLM. Quantitation of CBG metabolites using targeted mass spectrometry showed that the amount of cyclo-CBG produced is produced is ~100 fold higher than 6′,7′-epoxy-CBG. In the blood plasma samples, these metabolites are reduced after 2 h, which is potentially due to the secondary metabolism of the cyclo-CBG and 6′,7′-epoxy-CBG to form dihydroxy products. We further determined the enzymatic metabolism of CBG by CYPs. Kinetics of CBG metabolism shows that cyclo-CBG is the predominant product among all the CYPs and it is formed almost ~100 times more as compared to 6′,7′-epoxy-CBG..The substrate orientation near the heme as obtained from docking study shows that C-2′ and C-6′, are situated at a

distance of 6.35 Å and 8.60 Å from the oxo complex (Figure S1B (D)). Due to the shorter C2′ -oxo distance, the probability of C-H abstraction becomes more feasible from C2′ as compared to C6′, leading to higher 2′,3′-epoxy formation (which is subsequently converted to cyclo-CBG). Hence in our experiments, the extent of cyclo-CBG formation predominates over other product formation independent of the CYP involved in the study (SI notes on metabolism).

CYP2D6 and CYP3A4 are the major drug-metabolizing enzymes.[62] The extent of cyclo-CBG formation in CYP3A4 is comparable to that of CYP2C9, and the active site volume CYP3A4 (1226 $Å^3$)[63] is similar to CYP2C9. The sigmoidal graph for CYP3A4 suggesting more than one binding site. CBG binds near the B-C and F-G loop with Ser119 and Arg212 as the nearby residues and shares a common binding site with standard CYP3A4 drugs.[64] Four Phe residues (Phe108, Phe213, Phe215, and Phe304) situated within 5 Å distance from the ligand can bind CBG firmly near the heme through **π-π** stacking, therefore increasing the effectiveness of substrate metabolism. Change in CBG concentration affects the ratio of cyclo-CBG and 6′,7′-epoxy-CBG formation, as seen from Figure S5; however, it does not vary proportionally for all the CYPs. The ratio of cyclo:epoxy can be explained by close analysis of the kinetics plot from Figure 4. For CYP3A4 (Figure 4I and 4J), the cyclo-CBG product formation linearly increases till 35 μM concentration, whereas in this range, the 6′,7′-epoxy-CBG formation is almost static, leading to a higher ratio of cyclo-CBG formation in the initial phase of the reaction. However, following this, both these two metabolites show a steep rise leading to the appearance of plateau after 50 μM of CBG. A similar phenomenon is observed for CBG metabolism in the presence of 2C9 (Figure 4G and 4H). Hence the studies suggests a correlation between the rate of product formation in the *in vitro* and *in vivo* models.

With respect to their bioactivity, synthetic and plant derived cannabinoids have shown distinct differences in terms of receptor binding or physiological activity.[21,46,65,66] Herein, we find that CBG, sCBG and 2′,3′-dihydroxy-CBG shows concentration dependent reduction in IL-6 level thereby lowering pro-inflammatory activity. Among all the CBG based compounds carmagerol shows the highest reduction in the pro-inflammatory activity. On the other hand, CBG, carmagerol and 6′,7′-epoxy CBG show concentration dependent increase in IL-10 levels. In this study, CBG and 2′,3′-dihydroxy-CBG show maximum expression of the anti-inflammatory cytokines at 5 μM concentration. sCBG has a long hydrophobic chain and it does not significant bioactivity as compared to CBG metabolites having polar functional groups (either hydroxide or epoxide). On the other hand CBG is more anti-inflammatory compared to its di-hydroxy metabolite. From this study it can be inferred that optimum polarity and hydrophobicity at the prenyl chain is essential in regulating the inflammatory cytokines level in the BV2 microglial cell culture model.

CONCLUSION

CBG is a non-psychotropic cannabinoid that is a precursor of several cannabinoids. Due to its polypharmacology that makes it useful as a neuroprotective, anti-inflammatory, and antioxidant molecule, we study its fate when administered to animals. We perform *in vivo* metabolism using human liver microsomes and show that CBG is converted to

cyclo-CBG and 6′,7′-epoxy-CBG (Figure 6). These metabolites are novel, are also plant phytocannabinoids and have not been reported previously.

Supplementary Material

Refer to Web version on PubMed Central for supplementary material.

ACKNOWLEDGMENT

Financial support for this work was provided by the CCIL SEED grant, NCCIH R21 AT010761 to DS and AD, NCCIH R01 AT010757 to JH and NIGMS R01 GM1155884 to A.D. The Bruker 500-MHz NMR spectrometer was obtained with the financial support of the Roy J. Carver Charitable Trust, Muscatine, Iowa, USA. We also thank Dr. D. Olson and Dr. L. Zhu for NMR spectroscopic assistance and F. Sun for mass spectrometric assistance. We thank Dr. Lucas Li at the Roy J. Carver center for help with metabolomics.

REFERENCES

(1). Gagne SJ; Stout JM; Liu E; Boubakir Z; Clark SM; Page JE Identification of Olivetolic Acid Cyclase from Cannabis Sativa Reveals a Unique Catalytic Route to Plant Polyketides. Proc. Natl. Acad. Sci. 2012, 109 (31), 12811–12816. 10.1073/pnas.1200330109. [PubMed: 22802619]

(2). Akinola O; Ogbeche EO; Olumoh-Abdul HA; Alli-Oluwafuyi AO; Oyewole AL; Amin A; AbdulMajeed WI; Olajide OJ; Nafiu AB; Njan AA; Olorundare OE; Gbotosho GO Oral Ingestion of Cannabis Sativa : Risks, Benefits, and Effects on Malaria-Infected Hosts. Cannabis Cannabinoid Res. 2018, 3 (1), 219–227. 10.1089/can.2018.0043. [PubMed: 30498786]

(3). Makwana R; Venkatasamy R; Spina D; Page C The Effect of Phytocannabinoids on Airway Hyper-Responsiveness, Airway Inflammation, and Cough. J. Pharmacol. Exp. Ther. 2015, 353 (1), 169–180. 10.1124/jpet.114.221283. [PubMed: 25655949]

(4). Lowin T; Tingting R; Zurmahr J; Classen T; Schneider M; Pongratz G Cannabidiol (CBD): A Killer for Inflammatory Rheumatoid Arthritis Synovial Fibroblasts. Cell Death Dis. 2020, 11 (8), 714. 10.1038/s41419-020-02892-1. [PubMed: 32873774]

(5). Borrelli F; Fasolino I; Romano B; Capasso R; Maiello F; Coppola D; Orlando P; Battista G; Pagano E; Di Marzo V; Izzo AA Beneficial Effect of the Non-Psychotropic Plant Cannabinoid Cannabigerol on Experimental Inflammatory Bowel Disease. Biochem. Pharmacol. 2013, 85 (9), 1306–1316. 10.1016/j.bcp.2013.01.017. [PubMed: 23415610]

(6). Navarro G; Varani K; Reyes-Resina I; Sánchez de Medina V; Rivas-Santisteban R; Sánchez-Carnerero Callado C; Vincenzi F; Casano S; Ferreiro-Vera C; Canela EI; Borea PA; Nadal X; Franco R Cannabigerol Action at Cannabinoid CB1 and CB2 Receptors and at CB1–CB2 Heteroreceptor Complexes. Front. Pharmacol. 2018, 9 (632), 1–14. 10.3389/fphar.2018.00632. [PubMed: 29387012]

(7). Navarro G; Varani K; Lillo A; Vincenzi F; Rivas-Santisteban R; Raïch I; Reyes-Resina I; Ferreiro-Vera C; Borea PA; Sánchez de Medina V; Nadal X; Franco R Pharmacological Data of Cannabidiol- and Cannabigerol-Type Phytocannabinoids Acting on Cannabinoid CB1, CB2 and CB1/CB2 Heteromer Receptors. Pharmacol. Res. 2020, 159 (April), 104940. 10.1016/j.phrs.2020.104940. [PubMed: 32470563]

(8). Zagzoog A; Mohamed KA; Kim HJJ; Kim ED; Frank CS; Black T; Jadhav PD; Holbrook LA; Laprairie RB In Vitro and in Vivo Pharmacological Activity of Minor Cannabinoids Isolated from Cannabis Sativa. Sci. Rep. 2020, 10 (1), 1–13. 10.1038/s41598-020-77175-y. [PubMed: 31913322]

(9). Muller C; Morales P; Reggio PH Cannabinoid Ligands Targeting TRP Channels. Front. Mol. Neurosci. 2019, 11 (January), 1–15. 10.3389/fnmol.2018.00487.

(10). Cascio M; Gauson L; Stevenson L; Ross R; Pertwee R Evidence That the Plant Cannabinoid Cannabigerol Is a Highly Potent A2-Adrenoceptor Agonist and Moderately Potent 5HT1A Receptor Antagonist. Br. J. Pharmacol. 2010, 159 (1), 129–141. 10.1111/j.1476-5381.2009.00515.x. [PubMed: 20002104]

(11). Vernail VL; Bingaman SS; Silberman Y; Raup-Konsavage WM; Vrana KE; Arnold AC Acute Cannabigerol Administration Lowers Blood Pressure in Mice. Front. Physiol. 2022, 13 (May), 1–7. 10.3389/fphys.2022.871962.

(12). Nachnani R; Raup-Konsavage WM; Vrana KE The Pharmacological Case for Cannabigerol. J. Pharmacol. Exp. Ther. 2021, 376 (2), 204–212. 10.1124/jpet.120.000340. [PubMed: 33168643]

(13). Gugliandolo A; Pollastro F; Grassi G; Bramanti P; Mazzon E In Vitro Model of Neuroinflammation: Efficacy of Cannabigerol, a Non-Psychoactive Cannabinoid. Int. J. Mol. Sci. 2018, 19 (7), 1992. 10.3390/ijms19071992. [PubMed: 29986533]

(14). Nucci C; Bari M; Spanò A; Corasaniti M; Bagetta G; Maccarrone M; Morrone LA Potential Roles of (Endo)Cannabinoids in the Treatment of Glaucoma: From Intraocular Pressure Control to Neuroprotection. Prog. Brain Res. 2008, 173, 451–464. 10.1016/S0079-6123(08)01131-X. [PubMed: 18929127]

(15). Valdeolivas S; Navarrete C; Cantarero I; Bellido ML; Muñoz E; Sagredo O Neuroprotective Properties of Cannabigerol in Huntington's Disease: Studies in R6/2 Mice and 3-Nitropropionate-Lesioned Mice. Neurotherapeutics 2015, 12 (1), 185–199. 10.1007/s13311-014-0304-z. [PubMed: 25252936]

(16). Karas JA; Wong LJM; Paulin OKA; Mazeh AC; Hussein MH; Li J; Velkov T The Antimicrobial Activity of Cannabinoids. Antibiotics 2020, 9 (7), 406. 10.3390/antibiotics9070406. [PubMed: 32668669]

(17). Smeriglio A; Giofrè SV; Galati EM; Monforte MT; Cicero N; D'Angelo V; Grassi G; Circosta C Inhibition of Aldose Reductase Activity by Cannabis Sativa Chemotypes Extracts with High Content of Cannabidiol or Cannabigerol. Fitoterapia 2018, 127 (January), 101–108. 10.1016/j.fitote.2018.02.002. [PubMed: 29427593]

(18). Appendino G; Gibbons S; Giana A; Pagani A; Grassi G; Stavri M; Smith E; Rahman MM Antibacterial Cannabinoids from Cannabis Sativa: A Structure-Activity Study. J. Nat. Prod. 2008, 71 (8), 1427–1430. 10.1021/np8002673. [PubMed: 18681481]

(19). Huestis MA; Solimini R; Pichini S; Pacifici R; Carlier J; Busardò FP Cannabidiol Adverse Effects and Toxicity. Curr. Neuropharmacol. 2019, 17 (10), 974–989. 10.2174/1570159X17666190603171901. [PubMed: 31161980]

(20). Lemberger L; Martz R; Rodda B Comparative Pharmacology of Δ9 Tetrahydrocannabinol and Its Metabolite, 11 OH Δ9 Tetrahydrocannabinol. J. Clin. Invest. 1973, 52 (10), 2411–2417. 10.1172/JCI107431. [PubMed: 4729039]

(21). Khanolkar AD; Lu D; Ibrahim M; Duclos RI; Thakur GA; Malan TP; Porreca F; Veerappan V; Tian X; George C; Parrish DA; Papahatjis DP; Makriyannis A Cannabilactones: A Novel Class of CB2 Selective Agonists with Peripheral Analgesic Activity. J. Med. Chem. 2007, 50 (26), 6493–6500. 10.1021/jm070441u. [PubMed: 18038967]

(22). Dennis DG; Anand SD; Lopez AJ; Petrovčič J; Das A; Sarlah D Synthesis of the Cannabimovone and Cannabifuran Class of Minor Phytocannabinoids and Their Anti-Inflammatory Activity. J. Org. Chem. 2022, 87 (9), 6075–6086. 10.1021/acs.joc.2c00336. [PubMed: 35476908]

(23). Klein TW Cannabinoid-Based Drugs as Anti-Inflammatory Therapeutics. Nat. Rev. Immunol. 2005, 5 (5), 400–411. 10.1038/nri1602. [PubMed: 15864274]

(24). Morales P; Blasco-Benito S; Andradas C; Gómez-Cañas M; Flores JM; Goya P; Fernández-Ruiz J; Sánchez C; Jagerovic N Selective, Nontoxic CB 2 Cannabinoid o -Quinone with in Vivo Activity against Triple-Negative Breast Cancer. J. Med. Chem. 2015, 58 (5), 2256–2264. 10.1021/acs.jmedchem.5b00078. [PubMed: 25671648]

(25). Harvey DJ; Brown NK Comparative in Vitro Metabolism of the Cannabinoids. Pharmacol. Biochem. Behav. 1991, 40 (3), 533–540. 10.1016/0091-3057(91)90359-A. [PubMed: 1806943]

(26). Harvey DJ Stereospecific Elimination of Deuterium as a Method for Determining the Stereochemistry of a Number of Metabolites of the Tetrahydrocannabinols. Biol. Mass Spectrom. 1980, 7 (1), 28–34. 10.1002/bms.1200070107.

(27). Harvey DJ The Mass Spectra of the Trimethylsilyl Derivatives of the Hydroxy and Acid Metabolites of Δ1- and Δ6-tetrahydrocannabinol. Biol. Mass Spectrom. 1981, 8 (12), 579–588. 10.1002/bms.1200081205.

(28). Harvey DJ Mass Spectrometry of the Cannabinoids and Their Metabolites. Mass Spectrom. Rev. 1987, 6 (1), 135–229. 10.1002/mas.1280060104.

(29). Burris-Hiday SD; Scott EE Steroidogenic Cytochrome P450 17A1 Structure and Function. Mol. Cell. Endocrinol. 2021, 528 (October 2020), 111261. 10.1016/j.mce.2021.111261. [PubMed: 33781841]

(30). Arnold WR; Baylon JL; Tajkhorshid E; Das A Asymmetric Binding and Metabolism of Polyunsaturated Fatty Acids (PUFAs) by CYP2J2 Epoxygenase. Biochemistry 2016, 55 (50), 6969–6980. 10.1021/acs.biochem.6b01037. [PubMed: 27992998]

(31). Watanabe K; Narimatsu S; Matsunaga T; Yamamoto I; Yoshimura H A Cytochrome P450 Isozyme Having Aldehyde Oxygenase Activity Plays a Major Role in Metabolizing Cannabinoids by Mouse Hepatic Microsomes. Biochem. Pharmacol. 1993, 46 (3), 405–411. 10.1016/0006-2952(93)90516-Y. [PubMed: 8394082]

(32). Narimatsu S; Watanabe K; Matsunaga T; Yamamoto I; Imaoka S; Funae Y; Yoshimura H Cytochrome P-450 Isozymes in Metabolic Activation of Δ9-Tetrahydrocannabinol by Rat Liver Microsomes. Drug Metab. Dispos. 1990, 18, 843–948.

(33). Jiang R; Yamaori S; Takeda S; Yamamoto I; Watanabe K Identification of Cytochrome P450 Enzymes Responsible for Metabolism of Cannabidiol by Human Liver Microsomes. Life Sci. 2011, 89 (5–6), 165–170. 10.1016/j.lfs.2011.05.018. [PubMed: 21704641]

(34). Deiana S; Watanabe A; Yamasaki Y; Amada N; Arthur M; Fleming S; Woodcock H; Dorward P; Pigliacampo B; Close S; Platt B; Riedel G Plasma and Brain Pharmacokinetic Profile of Cannabidiol (CBD), Cannabidivarine (CBDV), Δ 9-Tetrahydrocannabivarin (THCV) and Cannabigerol (CBG) in Rats and Mice Following Oral and Intraperitoneal Administration and CBD Action on Obsessive-Compulsive Behav. Psychopharmacology (Berl). 2012, 219 (3), 859–873. 10.1007/s00213-011-2415-0. [PubMed: 21796370]

(35). Brierley DI; Samuels J; Duncan M; Whalley BJ; Williams CM Cannabigerol Is a Novel, Well-Tolerated Appetite Stimulant in Pre-Satiated Rats. Psychopharmacology (Berl). 2016, 233 (19–20), 3603–3613. 10.1007/s00213-016-4397-4. [PubMed: 27503475]

(36). Wilkinson GR Drug Metabolism and Variability among Patients in Drug Response. N. Engl. J. Med. 2005, 352 (21), 2211–2221. 10.1056/NEJMra032424. [PubMed: 15917386]

(37). Guengerich FP; Munro AW Unusual Cytochrome P450 Enzymes and Reactions. J. Biol. Chem. 2013, 288 (24), 17065–17073. 10.1074/jbc.R113.462275. [PubMed: 23632016]

(38). Hashimoto K Role of Soluble Epoxide Hydrolase in Metabolism of PUFAs in Psychiatric and Neurological Disorders. Front. Pharmacol. 2019, 10, 1–10. 10.3389/fphar.2019.00036. [PubMed: 30728774]

(39). Tomberg A; Pottel J; Liu Z; Labute P; Moitessier N Understanding P450-Mediated Bio-Transformations into Epoxide and Phenolic Metabolites. Angew. Chemie - Int. Ed. 2015, 54 (46), 13743–13747. 10.1002/anie.201506131.

(40). Hughes TB; Miller GP; Swamidass SJ Modeling Epoxidation of Drug-like Molecules with a Deep Machine Learning Network. ACS Cent. Sci. 2015, 1 (4), 168–180. 10.1021/acscentsci.5b00131. [PubMed: 27162970]

(41). DeLozier TC; Kissling GE; Coulter SJ; Dai D; Foley JF; Bradbury JA; Murphy E; Steenbergen C; Zeldin DC; Goldstein JA Detection of Human CYP2C8, CYP2C9, and CYP2J2 in Cardiovascular Tissues. Drug Metab. Dispos. 2007, 35 (4), 682–688. 10.1124/dmd.106.012823. [PubMed: 17220242]

(42). Radwan MM; ElSohly MA; Slade D; Ahmed SA; Khan IA; Ross SA Biologically Active Cannabinoids from High-Potency Cannabis Sativa. J. Nat. Prod. 2009, 72 (5), 906–911. 10.1021/np900067k. [PubMed: 19344127]

(43). Agrawal PK Natural Product Communications: Editorial. Nat. Prod. Commun. 2008, 3 (12), 1977–1980.

(44). Ren F-C; Wang L-X; Lv Y-F; Hu J-M; Zhou J Structure Revision of Four Classes of Prenylated Aromatic Natural Products Based on a Rule for Diagnostic 13 C NMR Chemical Shifts. J. Org. Chem. 2021, 86 (16), 10982–10990. 10.1021/acs.joc.0c02409. [PubMed: 33274942]

(45). Jamwal R; Topletz AR; Ramratnam B; Akhlaghi F Ultra-High Performance Liquid Chromatography Tandem Mass-Spectrometry for Simple and Simultaneous Quantification of Cannabinoids. J. Chromatogr. B 2017, 1048, 10–18. 10.1016/j.jchromb.2017.02.007.

(46). Node K; Huo Y; Ruan X; Yang B; Spiecker M; Ley K; Zeldin DC; Liao JK Anti-Inflammatory Properties of Cytochrome P450 Epoxygenase-Derived Eicosanoids. Science (80-.). 1999, 285 (5431), 1276–1279. 10.1126/science.285.5431.1276.

(47). Kraemer M; Madea B; Hess C Detectability of Various Cannabinoids in Plasma Samples of Cannabis Users: Indicators of Recent Cannabis Use? Drug Test. Anal. 2019, 11 (10), 1498–1506. 10.1002/dta.2682. [PubMed: 31407526]

(48). Go YY; Kim SR; Kim DY; Chae SW; Song JJ Cannabidiol Enhances Cytotoxicity of Anti-Cancer Drugs in Human Head and Neck Squamous Cell Carcinoma. Sci. Rep. 2020, 10 (1), 1–11. 10.1038/s41598-020-77674-y. [PubMed: 31913322]

(49). Arnold WR; Baylon JL; Tajkhorshid E; Das A Arachidonic Acid Metabolism by Human Cardiovascular CYP2J2 Is Modulated by Doxorubicin. Biochemistry 2017, 56 (51), 6700–6712. 10.1021/acs.biochem.7b01025. [PubMed: 29200270]

(50). Denisov IG; Grinkova YV; Camp T; McLean MA; Sligar SG Midazolam as a Probe for Drug–Drug Interactions Mediated by CYP3A4: Homotropic Allosteric Mechanism of Site-Specific Hydroxylation. Biochemistry 2021, 60 (21), 1670–1681. 10.1021/acs.biochem.1c00161. [PubMed: 34015213]

(51). Ziemys A; Kulys J Inhibition of Heme Peroxidase During Phenol Derivatives Oxidation. Possible Molecular Cloaking of the Active Center. Int. J. Mol. Sci. 2005, 6 (9), 245–256. 10.3390/i6090245.

(52). Sharma P; Murthy P; Bharath MMS Chemistry, Metabolism, and Toxicology of Cannabis: Clinical Implications. Iran. J. Psychiatry 2012, 7 (4), 149–156. [PubMed: 23408483]

(53). Ujváry I; Hanuš L Human Metabolites of Cannabidiol: A Review on Their Formation, Biological Activity, and Relevance in Therapy. Cannabis Cannabinoid Res. 2016, 1 (1), 90–101. 10.1089/can.2015.0012. [PubMed: 28861484]

(54). Arnold WR; Weigle AT; Das A Cross-Talk of Cannabinoid and Endocannabinoid Metabolism Is Mediated via Human Cardiac CYP2J2. J. Inorg. Biochem. 2018, 184, 88–99. 10.1016/j.jinorgbio.2018.03.016. [PubMed: 29689453]

(55). Szlenk CT; GC JB; Natesan S Does the Lipid Bilayer Orchestrate Access and Binding of Ligands to Transmembrane Orthosteric/Allosteric Sites of G Protein-Coupled Receptors? Mol. Pharmacol. 2019, 96 (5), 527–541. 10.1124/mol.118.115113. [PubMed: 30967440]

(56). Stock L; Hosoume J; Treptow W Concentration-Dependent Binding of Small Ligands to Multiple Saturable Sites in Membrane Proteins. Sci. Rep. 2017, 7 (1), 5734. 10.1038/s41598-017-05896-8. [PubMed: 28720769]

(57). Li W; Tang Y; Liu H; Cheng J; Zhu W; Jiang H Probing Ligand Binding Modes of Human Cytochrome P450 2J2 by Homology Modeling, Molecular Dynamics Simulation, and Flexible Molecular Docking. Proteins Struct. Funct. Bioinforma. 2008, 71 (2), 938–949. 10.1002/prot.21778.

(58). Wang A; Stout CD; Zhang Q; Johnson EF Contributions of Ionic Interactions and Protein Dynamics to Cytochrome P450 2D6 (CYP2D6) Substrate and Inhibitor Binding. J. Biol. Chem. 2015, 290 (8), 5092–5104. 10.1074/jbc.M114.627661. [PubMed: 25555909]

(59). Das A; Zhao J; Schatz GC; Sligar SG; Van Duyne RP Screening of Type I and II Drug Binding to Human Cytochrome P450–3A4 in Nanodiscs by Localized Surface Plasmon Resonance Spectroscopy. Anal. Chem. 2009, 81 (10), 3754–3759. 10.1021/ac802612z. [PubMed: 19364136]

(60). Kandel SE; Han LW; Mao Q; Lampe JN Digging Deeper into CYP3A Testosterone Metabolism: Kinetic, Regioselectivity, and Stereoselectivity Differences between CYP3A4/5 and CYP3A7. Drug Metab. Dispos. 2017, 45 (12), 1266–1275. 10.1124/dmd.117.078055. [PubMed: 28986474]

(61). Bonifacio A; Groenhof AR; Keizers PHJ; de Graaf C; Commandeur JNM; Vermeulen NPE; Ehlers AW; Lammertsma K; Gooijer C; van der Zwan G Altered Spin State Equilibrium in the T309V Mutant of Cytochrome P450 2D6: A Spectroscopic and Computational Study. JBIC J. Biol. Inorg. Chem. 2007, 12 (5), 645–654. 10.1007/s00775-007-0210-5. [PubMed: 17318599]

(62). Zhou S-F; Xue CC; Yu X-Q; Li C; Wang G Clinically Important Drug Interactions Potentially Involving Mechanism-Based Inhibition of Cytochrome P450 3A4 and the Role of Therapeutic Drug Monitoring. Ther. Drug Monit. 2007, 29 (6), 687–710. 10.1097/FTD.0b013e31815c16f5. [PubMed: 18043468]

(63). Yano JK; Wester MR; Schoch GA; Griffin KJ; Stout CD; Johnson EF The Structure of Human Microsomal Cytochrome P450 3A4 Determined by X-Ray Crystallography to 2.05-Å Resolution. J. Biol. Chem. 2004, 279, 38091–38094. 10.1074/jbc.C400293200. [PubMed: 15258162]

(64). Sevrioukova I Interaction of Human Drug-Metabolizing CYP3A4 with Small Inhibitory Molecules. Biochemistry 2019, 58 (7), 930–939. 10.1021/acs.biochem.8b01221. [PubMed: 30676743]

(65). Wrobleski ST; Chen P; Hynes J; Lin S; Norris DJ; Pandit CR; Spergel S; Wu H; Tokarski JS; Chen X; Gillooly KM; Kiener PA; McIntyre KW; Patil-Koota V; Shuster DJ; Turk LA; Yang G; Leftheris K Rational Design and Synthesis of an Orally Active Indolopyridone as a Novel Conformationally Constrained Cannabinoid Ligand Possessing Antiinflammatory Properties. J. Med. Chem. 2003, 46 (11), 2110–2116. 10.1021/jm020329q. [PubMed: 12747783]

(66). Carreira EM; Grether U; Sarott RC; Westphal MV; Pfaff P; Korn C; Sykes DA; Gazzi T; Brennecke B; Atz K; Weise M; Mostinski Y; Hompluem P; Koers E; Miljuš T; Roth NJ; Asmelash H; Vong MC; Piovesan J; Guba W; Rufer AC; Kusznir EA; Huber S; Raposo C; Zirwes EA; Osterwald A; Pavlovic A; Moes S; Beck J; Benito-Cuesta I; Grande T; De Martiń Esteban SR; Yeliseev A; Drawnel F; Widmer G; Holzer D; Van Der Wel T; Mandhair H; Yuan CY; Drobyski WR; Saroz Y; Grimsey N; Honer M; Fingerle J; Gawrisch K; Romero J; Hillard CJ; Varga ZV; Van Der Stelt M; Pacher P; Rg Gertsch J; McCormick PJ; Ullmer C; Oddi S; MacCarrone M; Veprintsev DB; Nazaré M Development of High-Specificity Fluorescent Probes to Enable Cannabinoid Type 2 Receptor Studies in Living Cells. J. Am. Chem. Soc. 2020, 142 (40), 16953–16964. 10.1021/jacs.0c05587. [PubMed: 32902974]

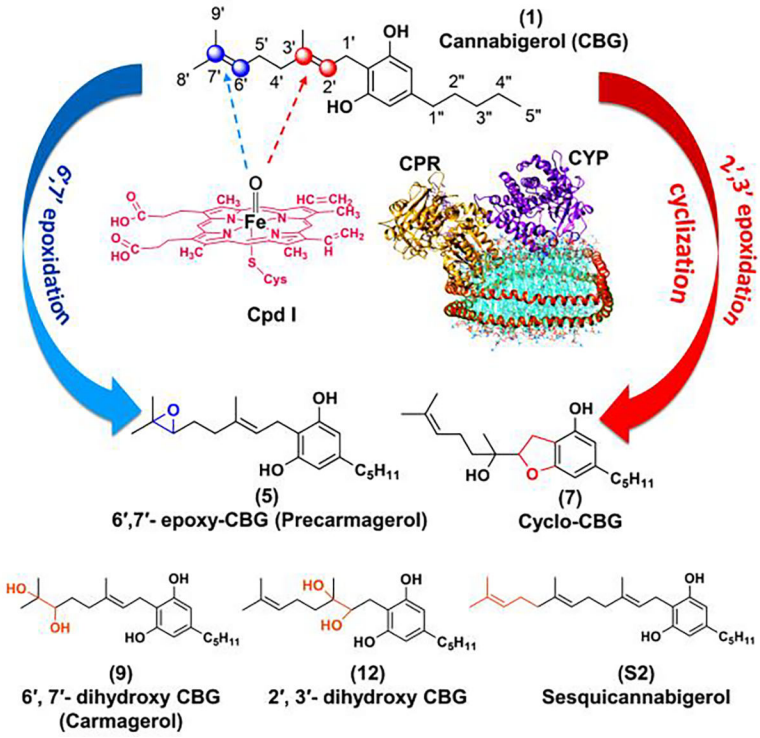

Figure 1. Schematic representation of metabolism of cannabigerol (CBG) in presence of Cytochrome P450 enzyme (CYP).

Epoxidation of CBG in presence of oxo-heme complex (prosthetic group of CYP, known as compound I or Cpd I) can occur either at the 2′,3′ position to give (7) cyclo-CBG or at 6′,7′ position to give (5) 6′,7′-epoxy-CBG. The sites of metabolism are shown in blue and red spheres. Along with these two, other CBG based compounds like: (9) 6′,7′-dihydroxy CBG (Carmagerol); (12) 2′,3′-dihydroxy CBG; and (S2) sesqicannabigerol have also been used in this work to study their anti-inflammatory properties. The protein nanodisc shown in this figure have: CYP (magenta), CPR (golden yellow) present in POPC/POPS nanodisc (cyan) which is bound by membrane scaffold protein MSPE3D1 (orange). For our study we have used CYP2J2, CYP2C8, CYP2C9, CYP2D6 and CYP3A4.

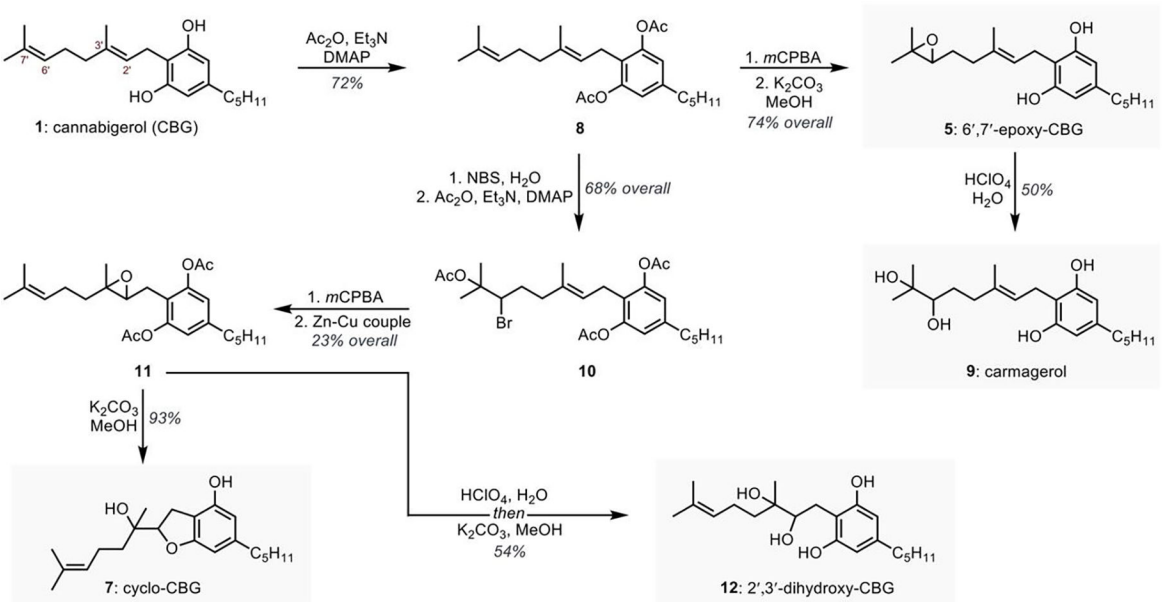

Figure 2.
Synthetic preparation of potential CBG (**1**) metabolites.

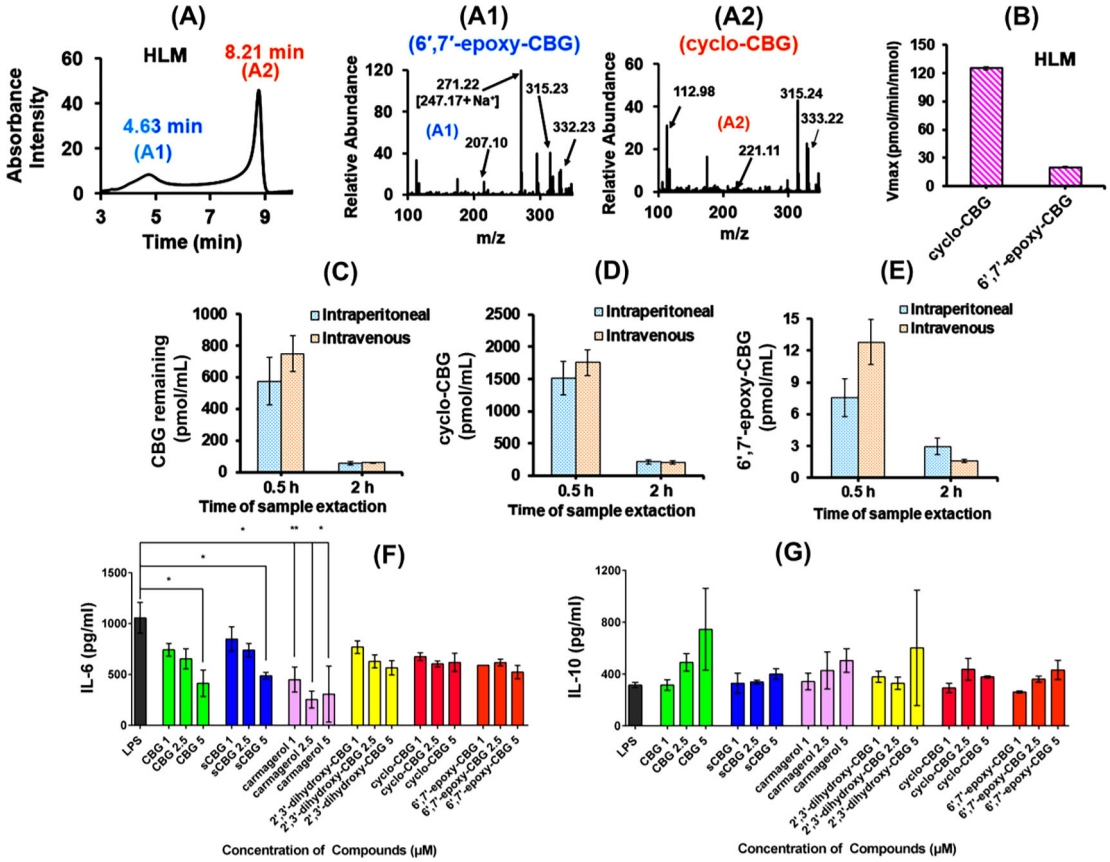

Figure 3. CBG Metabolism by Human Liver Microsome (HLM):

LC-UV chromatogram and MS fragmentation of CBG metabolites obtained from (A) Human liver microsome (HLM). Fragmentation pattern of (A1) 6′,7′-epoxy-CBG (**5**) eluted at 4.6 min (shown in blue) and (A2) cyclo-CBG (**7**) eluted at 8.2 min (shown in orange) from HLM. Fragments specific to cyclo- and 6′,7′-epoxy-CBG are marked in the figures. (B) Comparison of the extent of cyclo- and 6′,7′-epoxy-CBG formation in human liver microsome [HLM]. The rate is measured in pmol/min/nmol of protein and the concentration of substrate (CBG) used is 60 μM. ***In vivo* study:** CBG and CBG metabolite obtained from the blood plasma of female mice after CBG administration (dosage: 20 mg/kg) through intraperitoneal (IP) and intravenous mode (IV). Samples were taken after 0.5 h (blue bar) and 2 h (orange bar), and used for the analysis of the (C) remaining CBG, (D) cyclo-CBG, and (E) 6′,7′-epoxy-CBG. 200 μL of plasma samples were used for analysis. **Effect of CBG and its metabolites on biological systems.** (E) pro-inflammatory effect through IL-6 expression and (F) anti-inflammatory effect through IL-10 expression in presence of CBG, SCBG, cyclo-CBG, 6′,7′-epoxy-CBG and CBG diols at different concentration range. Data are represented as means ±SD of n=3 data points. *P < 0.5; **P < 0.01, one-way ANOVA

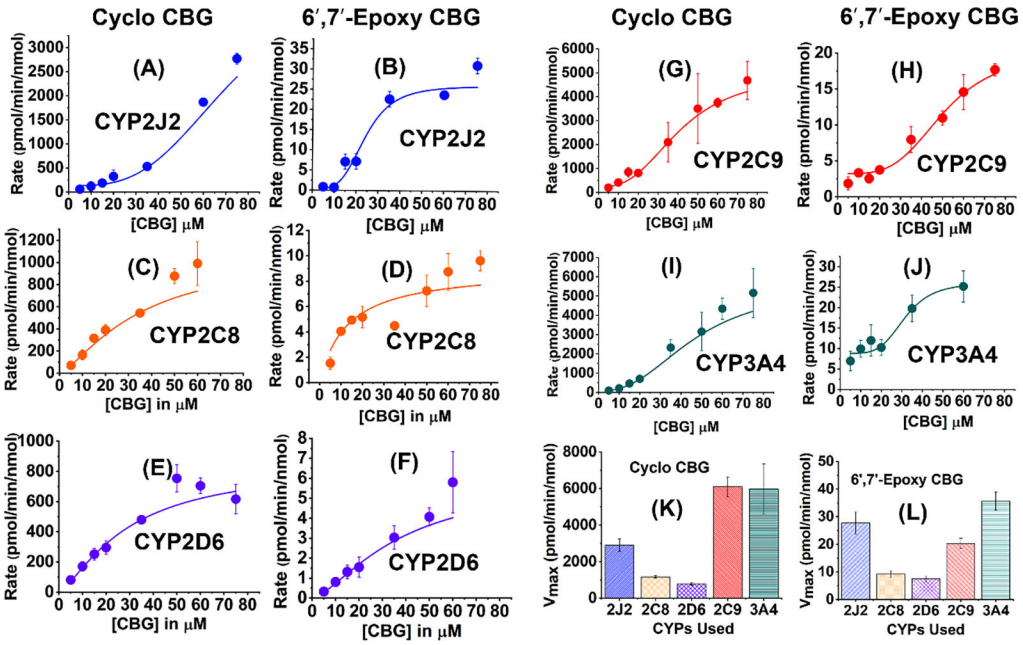

Figure 4. Metabolism of CBG in presence of CYPs:

CBG metabolism leads to the formation of cyclo-CBG (**7**) and 6′,7′-epoxy CBG (**5**). The kinetics of CBG metabolism are shown in the presence of CYP2J2 (blue), CYP2C8 (orange), CYP2D6 (purple), CYP2C9 (red), and CYP3A4 (green). Cyclo-CBG formation for all the CYPs are shown in (A), (C), (E), (G), (I) and 6′,7′-epoxy CBG in (B), (D), (F), (H), (J). **Comparison of product formation:** Maximum rate (Vmax) for (K) cyclo-CBG formation and 6′,7′-epoxy CBG formation are shown ion (K) and (l) respectively. Vmax is represented in pmol/min/nmol of protein in both the cases. The concentration of substrate (CBG) was varied 5–75 μM. Data has been fitted to either Michaelis-Menten or Hill equation and error bars represent ±SD

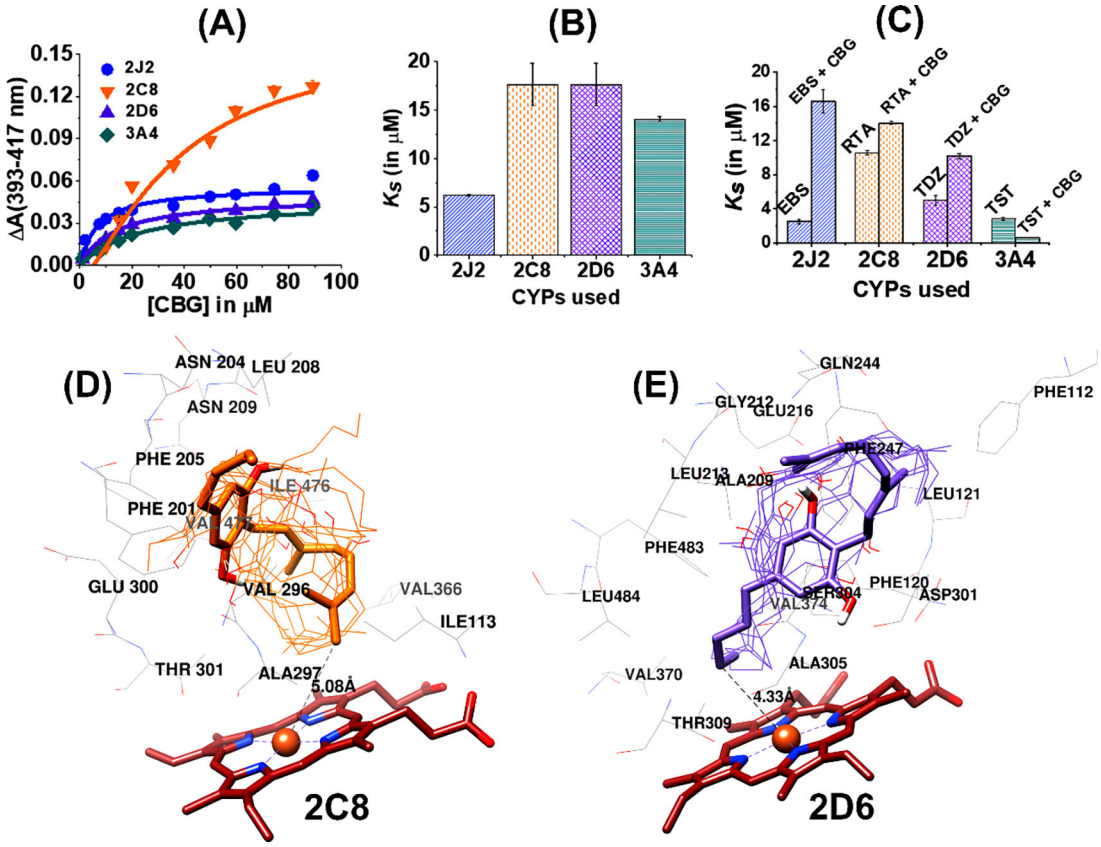

Figure 5. Binding of CBG to different CYPs.

(A) Soret titration binding curves for CBG with all four CYPs. 2J2 is shown in blue circles, 2C8 in orange inverted triangles, 2D6 in purple triangles and 3A4 in green diamonds. (B) Comparison of Ks (in μM) among four different CYPs. (C) Competitive binding study of ligands to different CYPs in presence and absence of CBG: Ebastine (EBS) with CYP 2J2 in the presence (EBS + CBG) and absence (EBS) of CBG; all *trans*-retinoic acid (RTA) with CYP 2C8 in the presence (RTA+CBG) and absence (RTA) of CBG; Thioridazine (TDZ) with CYP 2C8 in the presence (TDZ+CBG) and absence (TDZ) of CBG; Testosterone (TST) with CYP 3A4 in the presence (TST+CBG) and absence (CBG) of CBG. (G). All the binding spectra were fitted to a single binding isotherm. CBG was added incrementally from 0 to 90 μM. The change of absorbance (ΔA) from 393 to 417 nm was calculated for each titration and plotted CBG concentration (μM). Data were fitted with Origin Lab to the single binding isotherm to determine the Ks. All experiments were done in triplicate and data were produced from the means of three repeats (N=3). The error represents the standard error of the mean of three experiments. Comparison of Ks (in μM) among four different CYPs in the presence and absence of CBG. **Docking Study of CBG**: Protein-ligand docking between (D) CYP2C8 and (E) CYP2D6 with CBG (using AutoDock Vina) and the different docked poses of CBG are shown. The docked structures closest to Fe are shown as sticks models whereas the remaining CBG structures are shown as wires. The heme moiety is shown in brown. The nearby residues that are located within a distance of 5 Å are shown in the figures. The distance from Fe to CBG molecule indicates the closest distance between protein and ligand for various CYPs.

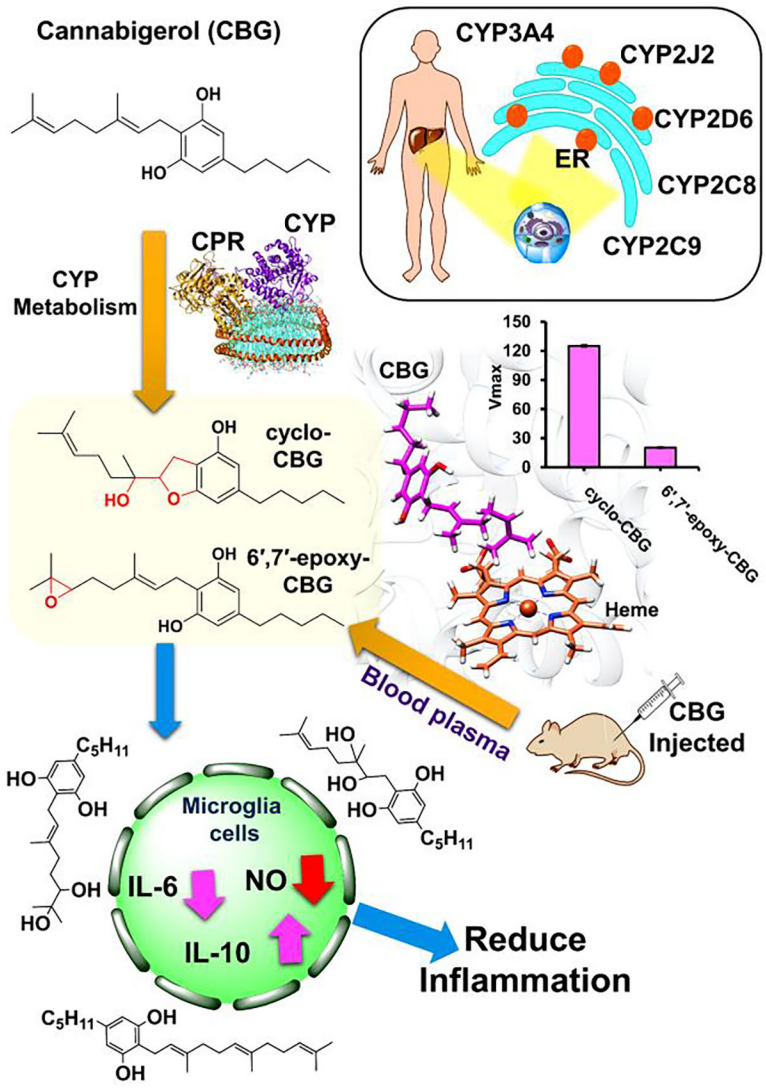

Figure 6.

Schematic representation of metabolism of cannabigerol (CBG) in presence of different CYPs (present in the liver endoplasmic reticulum : ER) to give 6′,7′-epoxy-CBG and cyclo-CBG as products. CYP (magenta), CPR (golden yellow) are present in POPC/POPS nanodisc (cyan) which is bound by membrane scaffold protein MSPE3D1 (orange). For this study we have selected CYPs which are mainly present in the liver and associated with drug metabolism. We have also carried out *in vivo* studies by injecting mice with CBG which also gives similar metabolites. CBG and its related compounds are bioactive and also found to have anti-inflammatory effect.